Oxidative stress transforms 3CLpro into an insoluble and more active form to promote SARS-CoV-2 replication

Liubing Du [a,1], Yanchun Xie [a,1], Kai Zheng [a,1], Niu Wang [a], Mingcheng Gao [a], Ting Yu [a], Liu Cao [a], QianQian Shao [d], Yong Zou [b], Wei Xia [c], Qianglin Fang [d], Bo Zhao [a], Deyin Guo [a], Xiaoxue Peng [a,**], Ji-An Pan [a,*]

[a] *The Center for Infection and Immunity Study and Molecular Cancer Research Center, School of Medicine, Shenzhen Campus of Sun Yat-sen University, No. 66, Gongchang Road, Guangming District, Shenzhen, Guangdong, 518107, China*
[b] *School of Pharmaceutical Sciences, Sun Yat-sen University, Guangzhou, 510006, China*
[c] *MOE Key Laboratory of Bioinorganic and Synthetic Chemistry School of Chemistry, Sun Yat-Sen University, Guangzhou, 510275, China*
[d] *School of Public Health (Shenzhen), Sun Yat-sen University, Guangming Science City, Shenzhen, 518107, China*

ARTICLE INFO

ABSTRACT

3CLpro is a key proteinase for SARS-CoV-2 replication and serves as an important target for antiviral drug development. However, how its activity is regulated intracellularly is still obscure. In this study, we developed a 3CLpro protease activity reporter system to examine the impact of various factors, including nutrient supplements, ions, pHs, or oxidative stress inducers, on 3CLpro protease activity. We found that oxidative stress could increase the overall activity of 3CLpro. Not altering the expression, oxidative stress decreased the solubility of 3CLpro in the lysis buffer containing 1% Triton-X-100. The Triton-X-100-insoluble 3CLpro was correlated with aggregates' formation and responsible for the increased enzymatic activity. The disulfide bonds formed between Cys85 sites of 3CLpro protomers account for the insolubility and the aggregation of 3CLpro. Besides being regulated by oxidative stress, 3CLpro impaired the cellular antioxidant capacity by regulating the cleavage of GPx1 at its N-terminus. This cleavage could further elevate the 3CLpro-proximate oxidative activity, favor aggregation and activation of 3CLpro, and thus lead to a positive feedback loop. In summary, we reported that oxidative stress transforms 3CLpro into a detergent-insoluble form that is more enzymatically active, leading to increased viral replication/transcription. Our study provided mechanistic evidence that suggests the therapeutic potential of antioxidants in the clinical treatment of COVID-19 patients.

1. Introduction

COVID-19 caused by SARS-CoV-2 spread worldwide, led to over 4 million deaths, and raised global health concerns (WHO). Despite researchers' unremitting efforts in developing anti-SARS-CoV-2 drugs, no effective drugs specific for SARS-CoV-2 are available in clinical therapy so far except remdesivir, whose efficacy needs more data to prove [1]. Thus, the drugs against SARS-CoV-2 are urgently needed. Although many chemicals effectively inhibit viral proteins' functions in test tubes, these inhibitory effects are attenuated drastically in live cells, indicating that the intracellular environment could affect these chemicals' functions [2,3].

Being one of the newest members infecting humans from the genus *Betacoronavirus* of the *Coronaviridae* family, SARS-CoV-2 uses a viral genomic RNA of 29.9 kb to encode a set of viral proteins for its proliferation [4,5]. More than nine open reading frames (ORFs) have been identified in the viral genome. ORF1ab, containing a coding region of ~21 kb at the 5′-proximal end of the genomic RNA, encodes the viral replicase polyproteins 1a and 1 ab (pp1a and pp1ab). ORF1ab is translated through the programmed −1 ribosomal frameshift, avoiding the translation termination by ORF1a′s stop codon [6]. The virus uses a discontinuous transcription and replication mechanism to generate its subgenomic RNAs [7]. Through these subgenomic RNAs, the ORFs at the 3′-proximal end of viral genome encode more than 8 viral proteins,

---

* Corresponding author.
** Corresponding author. School of Medicine, Guangming Science City, Shenzhen, 518107, China.
E-mail addresses: pengxx9@mail.sysu.edu.cn (X. Peng), panjan@mail.sysu.edu.cn (J.-A. Pan).
[1] Du Liubing, Xie Yanchun, and Zheng Kai contributed equally to this work.

including four structural proteins, spike (S), envelope (E), membrane (M), and nucleocapsid (N), and more than four accessory proteins whose functions await the further investigation [8].

The replicase polyproteins 1a and 1 ab are processed by two proteases, papain-like protease (PLpro) and chymotrypsin-like cysteine protease (3CLpro), resulting in 16 non-structural proteins (nsps) [8]. PLpro is located in nsp3 and is in charge of the cleavages at the cleavage sites (CSs) from nsp1 to nsp4, while 3CLpro is encoded by nsp5 and targets the CSs from nsp4 to nsp16. These cleavage processes play essential roles in maturing the viral replicase complex and making it fully functional. Thus, these two enzymes, especially 3CLpro, have attracted great attention and are considered prominent targets for anti-coronavirus drug development [2,8].

3CLpro, also known as main protease (Mpro), is highly conserved in coronaviruses and has no known homolog in humans [9]. Therefore, its specific inhibitors may impose a little adverse effect on patients. The 3D structures of 3CLpros from various coronaviruses have been resolved and helped delineate the mechanisms of its catalytic activity [10]. 3CLpro protomers form a homodimer, and each protomer is composed of three domains. His41 in domain I and Cys145 in domain II play essential roles in substrate-interaction and performing an enzymatic activity. Mutagenizing these two sites largely abolishes 3CLpro's proteolytic activity [11].

Numerous chemical inhibitors against 3CLpro have been developed by targeting its catalytic sites [12–15]. However, only a few of them have displayed a significant inhibitory effect on live viruses, and very few have been tested in clinical studies [15]. The inhibitors exhibit less efficacy on intracellular 3CLpro, compared with the 3CLpro purified for *in vitro* assays, suggesting that the intracellular environment may impact the behavior of 3CLpro, making it less sensitive to the inhibitors [2,3]. The intracellular factors could impact the protein sensitivity towards the inhibitors through various strategies, such as changing the protein's structure, which determines the protein functions [16]. Thus, we could investigate the alternation of 3CLpro structure by evaluating its intracellular activity and further explore the structural details of 3CLpro that are responsible for its sensitivity to the inhibitors by altering the key residues of 3CLpro.

In this study, we developed a reporter system to evaluate the proteolytic activity of 3CLpro in the cells. We investigated the activity of 3CLpro in the cells cultured in the media with various pHs, or that supplied with various nutrient supplements, ions, or oxidative stress inducers. We found that moderate oxidative stress could increase the overall activity of 3CLpro without the increase of overall 3CLpro expression. We revealed that oxidative stress decreased the solubility of 3CLpro in the lysis buffer containing 1% Triton-X-100. The Triton-X-100-insoluble 3CLpro was correlated with aggregates' formation. The disulfide bonds formed between C85 sites of two 3CLpro protomers account for the insolubility of 3CLpro. 3CLpro could impair the cellular capacity of antioxidant response by triggering the cleavage of glutathione peroxidase 1 (GPx1) at GE↓PV in its N-terminus. This cleavage led to the increased oxidative environment locally, which may further favor the formation of disulfide bonds and aggregation of 3CLpro. In summary, we uncovered that oxidative stress promoted viral replication by transforming 3CLpro into an insoluble and more active form, which likely facilitates 3CLpro's escape from the trap of inhibitors in the cells.

2. Results

2.1. The design and construction of 3CLpro activity reporter system

To monitor the activity of 3CLpro in cells, we designed and generated a 3CLpro activity reporter system, which aimed to sensitively, dynamically, and quantitatively detect the activity of 3CLpro. We employed firefly luciferase as the reporter gene for the system. Paired with renilla luciferase (RL-TK), the firefly luciferase is widely used to detect the activities of various biological processes [17]. To attain a stable basal

line and relatively low background, we fused the firefly luciferase with tandem ubiquitin proteins, leading to its degradation in the proteasome. We found that four tandem repeats of ubiquitin coding sequences (Ub4) could efficiently induce the degradation of firefly luciferase, consistent with the previous studies [18], and the degradation was sensitive to the inhibition of proteasome activity (Fig. 1A).

To correlate the firefly luciferase activity with the 3CLpro activity, we inserted CS of 3CLpro between Ub4 and firefly luciferase. Because no human homolog of 3CLpro was identified so far, CS is most likely to be recognized and cleaved by 3CLpro [9]. The cleavage by 3CLpro at CS detaches the firefly luciferase from Ub4, thus decreasing the degradation of firefly luciferase, which could be measured to reflect the activity of 3CLpro (Fig. 1B).

Eleven CSs in ORF1ab are recognized and cleaved by 3CLpro. Without knowing which was more potent, we sought to design a CS with consensus amino acid residues. By analyzing amino acid residues upstream and downstream of glutamine, where 3CLpro separates the two neighboring nsps, we designed a CS, with the glutamine flanked by 10 consensus amino acid residues, for our reporter system (Fig. 1C). We inserted the designed CS between Ub4 and firefly luciferase genes (Ub4-CS-Luci) and found the insertion did not influence the ubiquitin-mediated degradation of firefly luciferase (Fig. 1D).

We expressed 3CLpro, Ub4-CS-Luci, and pRL-TK in HEK293T cells (designated as 3CLpro activity reporter system) and found that 3CLpro significantly increased the readings of firefly luciferase activity in a dosage-dependent manner (Fig. 1E). To confirm that this effect was CS-dependent, we mutated Q of CS to N and found this mutation completely abolished the activity of firefly luciferase induced by 3CLpro (Fig. 1F). To further confirm this effect was the 3CLpro protease activity-dependent, we compared the promoting effect of WT 3CLpro on the luciferase activity with various mutant 3CLpros. As predicted, 3CLpro with H41A, C145S, or H163A [11], the enzymatic inactive mutants, failed to rescue the firefly luciferase activity, while 3CLpro with M162A, the mutant with increased enzymatic activity, not only rescued but also even increased the activity of firefly luciferase compared with WT 3CLpro [19] (Fig. 1G). 3CLpro with G11A, the mutant losing the ability to form the dimer, also showed lower activity compared with WT [20] (Fig. 1G).

To rule out the possibility that the cleavage was the designed CS-specific, we compared three various CSs cleaved by PLpro and 11 various CSs cleaved by 3CLpro in ORF1ab with the designed CS by us (Fig. 1C and H). All the viral CSs were inserted between Ub4 and firefly luciferase, and the 3CLpro activity assays were performed as aforementioned. Like the designed CS, 3CLpro cleaved the CSs from nsp4 to nsp16, but the cleavage efficiency at different cleavage sites varied (Fig. 1I). Compared with most of the viral CSs, the designed CS was more potent (Fig. 1I). To investigate whether a tandem repeat of CSs could improve the cleavage efficiency, we inserted 2 or 3 repeats of designed CSs between Ub4 and firefly luciferase and observed that one CS was sufficient for the recognition and cleavage by 3CLpro (Fig. 1J).

2.2. Oxidative stress increases the activity of 3CLpro

To further investigate whether and how the activity of 3CLpro is regulated in the mammalian cells, we cultured the cells, transfected with the 3CLpro activity reporter system, in the cell culture medium deprived of various nutrients, such as serum (S), essential amino acids (EAA), non-essential amino acids (NEAA), glutamine (Q), and glucose (Glc). None of these nutrient deprivations had a marked impact on the activity of 3CLpro except that EAA deprivation increased the activity of 3CLpro to some extent (Figs. S1A and S1B).

Ions play essential roles in the activity of many proteases. We cultured the cells, which were transfected with the 3CLpro activity reporter system, in the medium with the additional supplement of various ions, including calcium, magnesium, or manganese ions. We observed that manganese ion increased the activity of 3CLpro markedly (Fig. 2A),
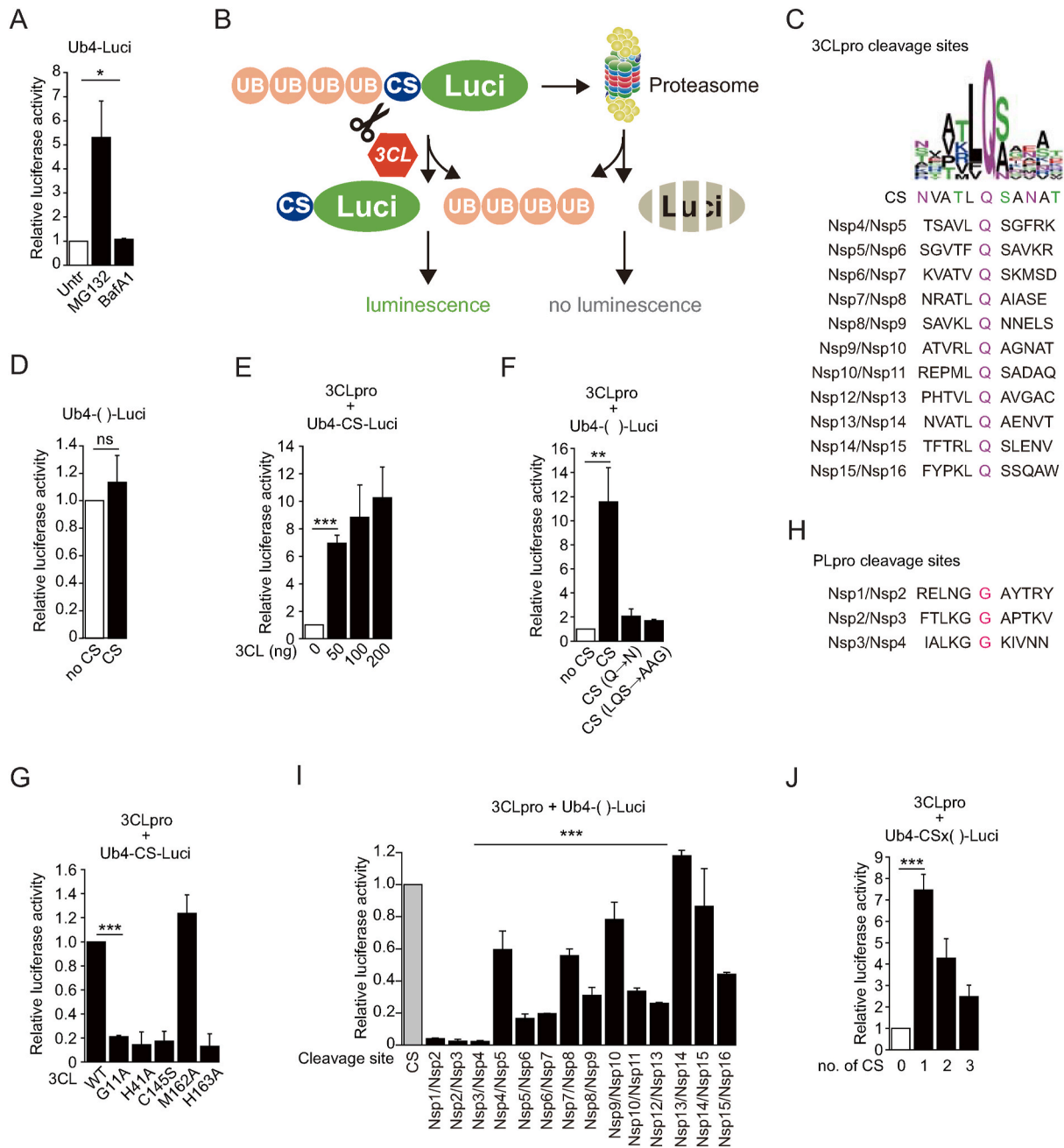
Fig. 1. Construction of 3CLpro activity reporter system.

(A) HEK293T cells were transfected with Ub4-Luci and pRL-TK. 24 h post-transfection, the cells were left untreated or treated with MG132 at 0.5 μM or Bafilomycin A1 (Baf A1) at 0.05 μM for 12 h. The cells were collected, and the lysates were subjected to Dual-Luciferase® Reporter (DLR™) Assay. Note that MG132 retained the luciferase activity through the inhibition of Ub4 mediated degradation. (B) Schematic illustration of 3CLpro activity reporter system. Four tandem ubiquitins mediate the degradation of luciferase through the proteasome pathway. The cleavage site of 3CLpro is inserted between four tandem ubiquitins and luciferase. 3CLpro recognizes and cuts the cleavage site and separates luciferase from four tandem ubiquitins. The luciferase activity could be quantified and reflects the 3CLpro activity. (C) Eleven cleavage sequences of 3CLpro were analyzed using WEBLOGO, and the consensus sequence was designated as CS. (D) HEK293T cells were transfected with Ub4-Luci or Ub4-CS-Luci and pRL-TK. 24 h post-transfection, the cells were collected, and the lysates were subjected to Dual-Luciferase® Reporter (DLR™) Assay. (E) HEK293T cells were transfected with Ub4-CS-Luci, pRL-TK and 3CLpro with indicated amounts. 24 h post-transfection, the cells were collected, and the lysates were subjected to Dual-Luciferase® Reporter (DLR™) Assay. (F) HEK293T cells were transfected with 3CLpro, pRL-TK, and Ub4-CS-Luci or Ub4-CS-Luci with indicated mutations. 24 h post-transfection, the cells were collected, and the lysates were subjected to Dual-Luciferase® Reporter (DLR™) Assay. (G) HEK293T cells were transfected with pRL-TK, Ub4-CS-Luci, and 3CLpro WT or various mutants. 24 h post-transfection, the cells were collected, and the lysates were subjected to Dual-Luciferase® Reporter (DLR™) Assay. (H) 3 cleavage sequences of PLpro were analyzed. (I) HEK293T cells were transfected with 3CLpro, pRL-TK and Ub4-CS-Luci or Ub4-Luci inserted with indicated various viral cleavage sequences. 24 h post-transfection, the cells were collected, and the lysates were subjected to Dual-Luciferase® Reporter (DLR™) Assay. (J) HEK293T cells were transfected with 3CLpro, pRL-TK, and Ub4-Luci inserted with different numbers of CS. 24 h post-transfection, the cells were collected, and the lysates were subjected to Dual-Luciferase® Reporter (DLR™) Assay. The data represent one of three independent experiments with similar results; error bars represent the mean ± s.e.m. A two-tailed unpaired Student's t-test or one-way ANOVA with Bonferroni post-test correction was used to analyze the significance; *P < 0.05, **P < 0.01, ***P < 0.001.
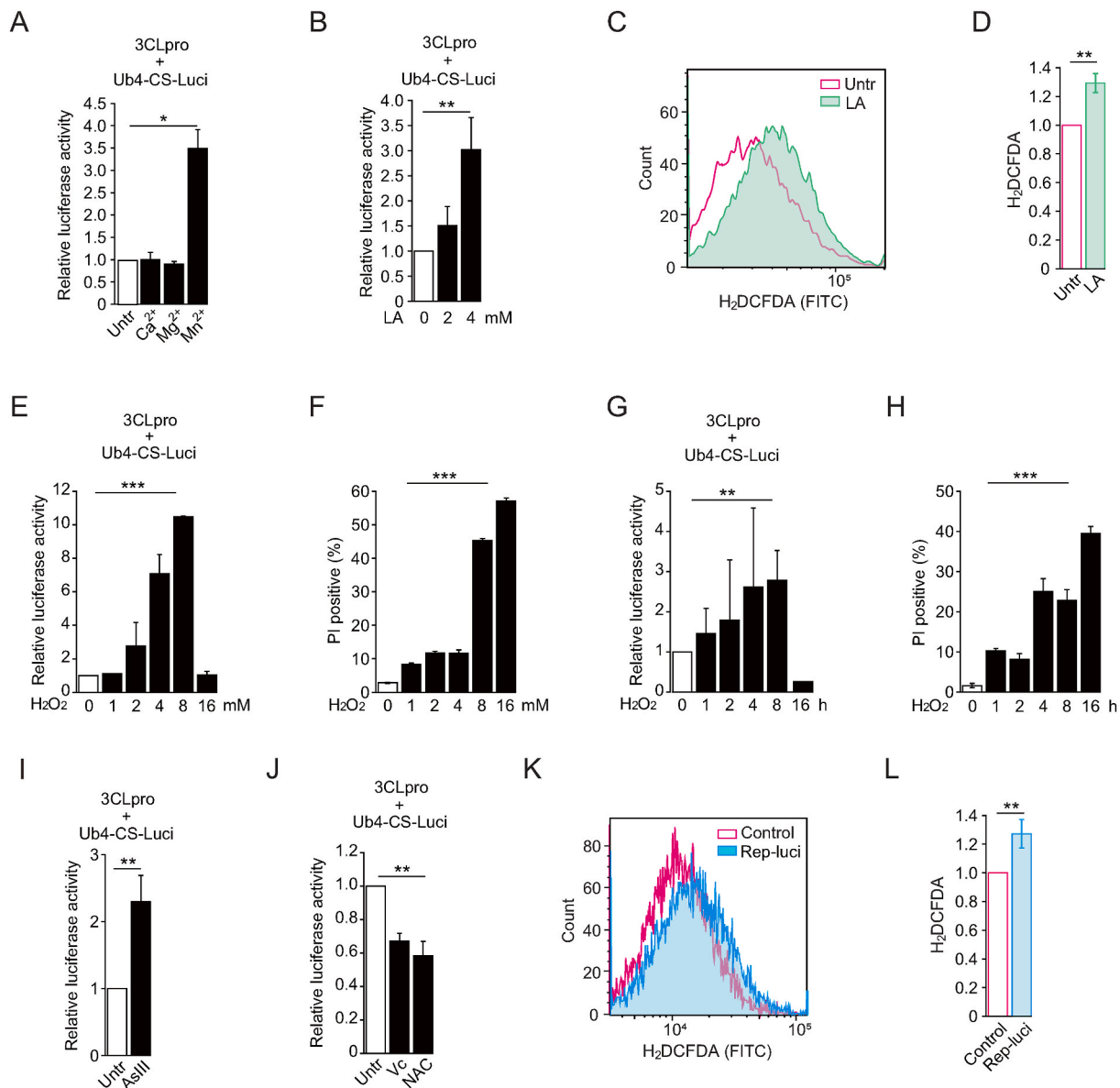
Fig. 2. H_2O_2 promoted the activity of 3CLpro in cells.

The combination of 3CLpro, Ub4-CS-Luci, and pRL-TK was designated as 3CLpro activity reporter system. HEK293T cells, transfected with a 3CLpro activity reporter system, were left untreated or treated with various ions for 16 h (A), indicated concentrations of lactic acid for 16 h (B), indicated concentrations of H_2O_2 for 2 h (E), and 2 mM of H_2O_2 for indicated durations (G). The cells were collected, and the lysates were subjected to Dual-Luciferase® Reporter (DLR™) Assay. (C) and (D) HEK293T cells were left untreated or treated with 4 mM of LA for 16 h. After being stained with 5 μM H_2DCFDA (FITC) for 30 min, the cells were collected and analyzed using CytoFLEX cytometry. After the H_2O_2 treatment with various concentrations (F) and durations (H), the cells, including suspended cells, were collected and stained with propidium iodide. The percentages of PI-positive cells were analyzed using CytoFLEX cytometry. (I) and (J) HEK293T cells, transfected with 3CLpro activity reporter system, were left untreated or treated with 5 μM arsenite, 8 mM vitamin C and 16 mM NAC. The cells were collected, and the lysates were subjected to Dual-Luciferase® Reporter (DLR™) Assay. (K) and (L) HEK293T cells were left untransfected or transfected with pBAC-nCoV-Replicon (Rep). 72 h post-transfection, the cells were stained with 5 μM H_2DCFDA (FITC) for 30 min. The cells were collected and analyzed using CytoFLEX cytometry. The data represent one of three independent experiments with similar results; error bars represent the mean ± s.e.m. A two-tailed unpaired Student's t-test or one-way ANOVA with Bonferroni post-test correction was used to analyze the significance; *P < 0.05, **P < 0.01, ***P < 0.001.

which was not due to the direct impact of manganese ion on the activity of Ub4-CS-Luci (Fig. S1C). Since no research has identified the binding sites of manganese ion in 3CLpro purified from the bacteria, manganese ion likely indirectly regulated the activity of 3CLpro through an unknown mechanism.

The serum samples from the patients, who were infected with SARS-CoV-2, contained a higher concentration of lactic acid, resulting in an acidic microenvironment [21]. To explore whether lactic acid could impact the activity of 3CLpro, we cultured the cells, which were transfected with the 3CLpro activity reporter system, in the medium with

lactic acid. The results showed that lactic acid increased the activity of 3CLpro in a dosage-dependent manner (Fig. 2B), which was not due to the direct impact of lactic acid on the activity of Ub4-CS-Luci (Fig. S1D). The lactic acid could decrease the pH of cell culture medium to around 6 [22]. We examined whether the cell culture medium with different pHs impacted the activity of 3CLpro. We cultured the cells, which were transfected with the 3CLpro activity reporter system, in the medium with various pHs (from 8 to 5). The results showed that pH 6.0 increased the 3CLpro activity drastically, while pH 5.0 failed to do so (Fig. S1E). The acidic stress in the medium at pH 5.0 likely went beyond the buffer

capacity of 293T cells and thus led to the obvious morphologic changes of 293T cells, consistent with the previous reports [23]. Besides the induction of acidic microenvironment, lactic acid could alter the intracellular oxidative activity, consistent with the previous findings [23–25] (Fig. 2C and D).

We sought to determine whether lactic acid increased the activity of 3CLpro by upregulating oxidative activity. We treated the cells, transfected with the 3CLpro activity reporter system, with H_2O_2 to stimulate the oxidative stress. The result of the 3CLpro activity assay showed that H_2O_2 treatment markedly increased the activity of 3CLpro in HEK293T cells (Fig. 2E and G), Vero E6 cells (Fig. S2J), A549 cells (Fig. S2K), and Jurkat cells (Fig. S2L), and the H_2O_2 treatment-induced activity of 3CLpro was correlated with dosages and the duration of H_2O_2 treatment (Fig. 2E and G), which was not due to the direct impact of H_2O_2 on the activity of Ub4-CS-Luci (Fig. S1F). The increase in the 3CLpro activity was diminished when cell deaths were induced by high dosage and long duration of H_2O_2 treatment (Fig. 2F and H). Consistent with the effect of H_2O_2 treatment, arsenite As(III), an oxidative stress inducer, also exhibited the ability to improve the 3CLpro activity (Fig. 2I) [26]. To investigate whether the basal level of oxidative activity could impact the protease activity of 3CLpro, we used the known antioxidants, vitamin C (Vc) and N-acetyl-L-cysteine (NAC), to treat the cells transfected with 3CLpro activity reporter system. Contrary to oxidative stress inducers, Vc and NAC significantly decreased the protease activity of 3CLpro (Fig. 2J), which was not due to the direct impact of Vc and NAC on the activity of Ub4-CS-Luci (Fig. S1G).

Next, we sought to determine whether viral infection could lead to increased oxidative stress. Because it raises the biosafety concerns to measure the ROS level in the cells infected with live SARS-CoV-2, we transfected the cells with the replicon plasmid of SARS-CoV-2 (Rep) to simulate the process of viral replication and transcription inside the cells without the generation of progeny viruses [27] (Fig. S1H). The cells were stained with H_2DCFDA and analyzed on flow cytometry. Compared with cells transfected with vector, the cells expressing the replicon of SARS-CoV-2 exhibited the increased overall intracellular oxidative activity (Fig. 2K and L), consistent with the recent finding that SARS-CoV2 infection impairs redox function [28].

Collectively, we found that the viral replication increased the intracellular oxidative activity, which likely subsequently increases the 3CLpro activity.

2.3. The amount of Triton-X-100-insoluble 3CLpro is correlated with the activity of 3CLpro

The mutation of M162A increased the activity of 3CLpro (Fig. 1G). To explore whether this activity increase was due to the increased protein level of 3CLpro, we lysed the cells, which were transfected with WT 3CLpro or 3CLpro containing different mutations, with DISC IP buffer containing 1% Triton-X-100 and subjected the lysates to western blotting (WB). The results showed that the expression level of M162A mutant was lower than WT and other mutants (Fig. 3A). The DISC IP buffer's dissolving condition is similar to that used for protein purification in vitro, and it is widely used for detecting the expression of proteins and pull-down assays. In our laboratory practice, we noticed that DISC IP buffer could not dissolve all the components of cells. To examine the possibility that 3CLpro was partially dissolved in the DISC IP buffer, we lysed the cells in RIPA buffer containing 1% SDS, which could dissolve nearly all the components of the cells, and subjected the lysates to WB analysis. The WB results showed that the expression difference between M162A mutant and WT in the lysates prepared with
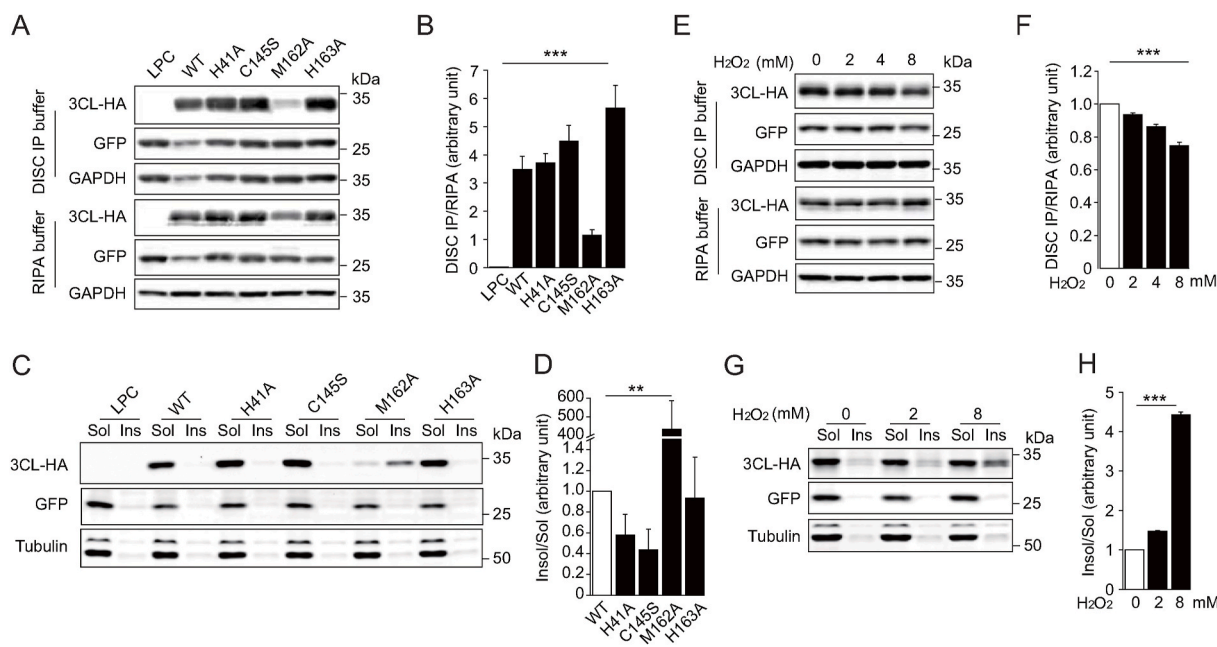
Fig. 3. H_2O_2-treatment altered the 3CLpro solubility in DISC IP buffer.
(A) HEK293T cells were transfected with WT 3CL-HA or 3CL-HA with indicated mutations and GFP, which was used as the internal control for transfection. The cells were collected, split into two portions, and lysed separately with DISC IP buffer and RIPA buffer. The lysates were subjected to WB analysis. The intensities of various bands were quantified using Image Studio™ Lite Software, and the intensity of each 3CL-HA band was normalized with that of related GFP. (B) The ratios of various 3CL-HA proteins lysed in DISC IP buffer to that in RIPA buffer were presented. The cell lysates in DISC IP buffer from (A) were centrifugated at 12,000 g for 10 min at 4 °C. The supernatants were designated as soluble fractions. The pellets were resuspended in RIPA buffer with sonication and designated as insoluble fractions. Same as (A) and (B), the soluble and insoluble lysates were analyzed using WB (C), and the ratios of soluble fractions to insoluble fractions were presented (D). HEK293T cells, transfected with 3CL-HA, were left untreated or treated with indicated concentrations of H_2O_2 for 2 h. Same as (A) and (B), the cell lysates were analyzed using WB (E), and the ratios of 3CL-HA proteins lysed in DISC IP buffer to that in RIPA buffer were presented (F). Same as (C) and (D), the soluble and insoluble lysates of cells from (E) were analyzed using WB (G), and the ratios of soluble fractions to insoluble fractions were presented (H). The data represent one of three independent experiments with similar results; error bars represent the mean ± s.e.m. A two-tailed unpaired Student's t-test or one-way ANOVA with Bonferroni post-test correction was used to analyze the significance; *P < 0.05, **P < 0.01, ***P < 0.001.

RIPA buffer is smaller than that with DISC IP buffer, indicating that 3CLpro M162A could be more DISC IP buffer-insoluble than WT 3CLpro (Fig. 3A and B).

To further confirm that the insoluble components contained the 3CLpro, we dissolved the DISC IP buffer-insoluble pellet with RIPA buffer and subjected the samples to WB analysis. The results showed that most of 3CLpro M162A was in the insoluble portion (Fig. 3C and D). Compared with WT 3CLpro, both total and soluble amounts of M162A mutant proteins were lower (Fig. 3A). This difference was not caused by loading different amounts of cell lysates, transfection efficiency variations, or contaminations between soluble and insoluble portions, because the total protein amounts in soluble and insoluble samples were comparable, and control protein GFP was not detected in the insoluble samples (Figs. S2A, 3C, and 3D). Considering that M162A mutant performed a higher enzymatic activity (Fig. S2S and S2T), we speculated that insoluble 3CLpro likely possessed an unexpected enzymatic activity.

As aforementioned, H_2O_2 treatment increased 3CLpro activity. To investigate the reason for the increased 3CLpro activity, we firstly analyzed the expression level of 3CLpro by dissolving the cells in both DISC IP buffer and RIPA buffer. The WB results showed that in RIPA buffer, 3CLpro protein amounts were similar, while in DISC IP buffer, the amounts decreased with the H_2O_2 treatment, indicating that H_2O_2 treatment could alter the solubility of 3CLpro (Fig. 3E and F). We dissolved insoluble components in the RIPA buffer with sonication and subjected them to WB analysis. As predicted, we observed that H_2O_2 treatment markedly increased the insoluble portion of 3CLpro in a dosage-dependent manner (Fig. 3G and H). Furthermore, we confirmed that H_2O_2 treatment could increase the insoluble portion of 3CLpro in Vero E6 cells (Fig. S2M and S2N), A549 cells (Fig. S2O and S2P), and Jurkat cells (Fig. S2Q and S2R). Considering that H_2O_2 treatment increased both the activity and insolubility of 3CLpro, we hypothesized that insoluble 3CLpro retained the protease function and performed it even in a stronger manner.

We investigated the correlation of the insolubility induced by various conditions with the altered 3CLpro activities. We observed that the manganese ion (Figs. S2B and S2C), lactic acid (Figs. S2D and S2E), low pH (Figs. S2F and S2G), and As(III) (Figs. S2H and S2I), which could promote the 3CLpro activity, significantly increased the insolubility of 3CLpro.

2.4. H_2O_2 alters the solubility of 3CLpro through the induction of aggregation

The aggregation decreases the solubility of proteins and increases the size of protein complexes [26]. To explore whether 3CLpro is involved in the aggregation, we determined the size of protein complexes containing 3CLpro by using gel filtration. Due to the technical limitations in characterizing the molecular weight of insoluble proteins, we sought to investigate the distribution of soluble 3CLpro proteins in various elution
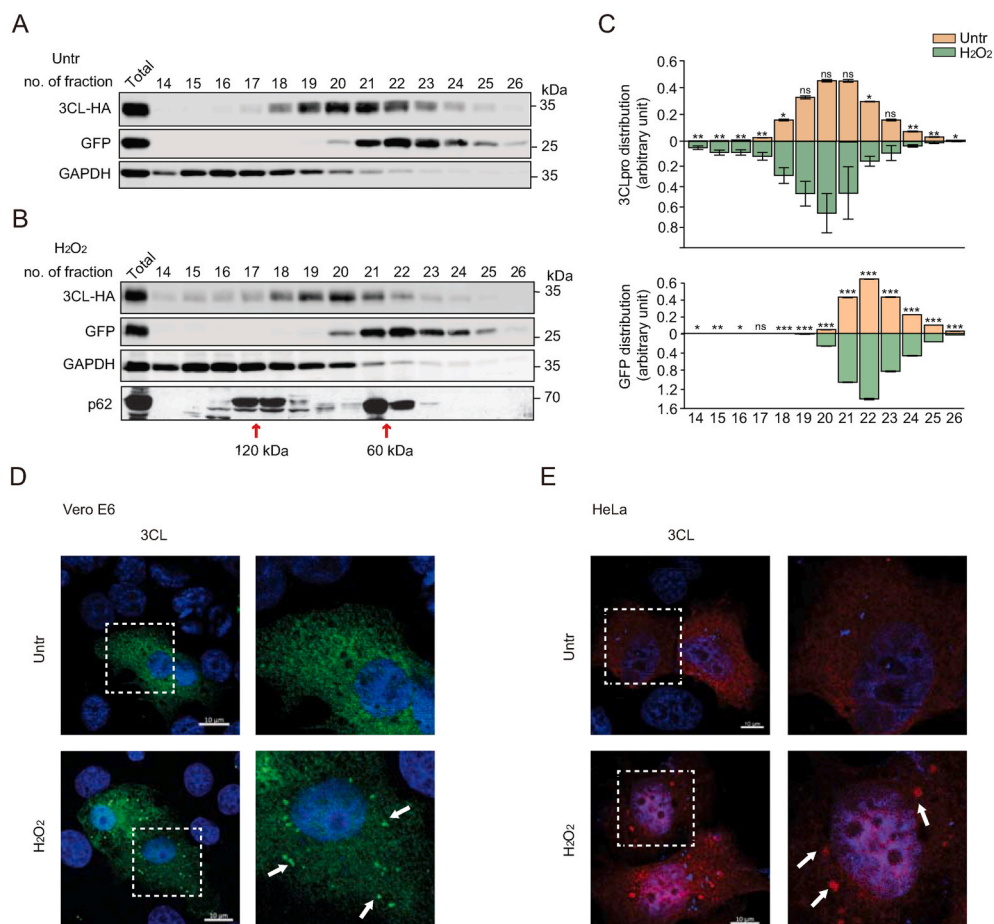
Fig. 4. H_2O_2-treatment induced the aggregation of 3CLpro.

HEK293T cells, transfected with WT 3CL-HA and GFP, were left untreated (A) or treated with 2 mM H_2O_2 for 2 h (B). The cells were lysed in DISC IP buffer, and the cell lysates were cleared with centrifugation at 12,000 g for 20 min at 4 °C to obtain the soluble fractions. After filtration through a 0.45-μm-pore-size filter, the soluble fractions were loaded onto a Superdex 200 10/300 GL column. The samples were eluted with Elution buffer (50 mM Tris-HCl, pH 7.5, 150 mM NaCl) and collected in 0.5 mL of elutes per fraction. The elutes were subjected to WB analysis with indicated antibodies. p62 protein, which distributes mainly in the fraction of 60 kDa as a monomer and 120 kDa as a dimer, was used as an indicator for molecular weight [38]. The intensities of 3CLpro and GFP bands in (A) and (B) were quantified using Image Studio™ Lite Software. (C) The relative amounts of 3CLpro or GFP were obtained by normalizing the intensities of 3CLpro or GFP in each fraction with that in the soluble fractions. Note that H_2O_2 treatment triggered more 3CLpro, not GFP, distribution in the fractions related to protein complexes with high molecular weight. Vero E6 (D) and HeLa (E) cells, transfected with 3CL-HA, were left untreated or treated with 2 mM H_2O_2 for 2 h. The cells were fixed, permeabilized, and subjected to IF assay. The cells were observed under Zeiss Confocal LSM800 Microscope. Note that H_2O_2 treatment induced the aggregate formation of 3CLpro. The data represent one of three independent experiments with similar results; error bars represent the mean ± s.e.m. A two-tailed unpaired Student's t-test was used to analyze the significance; *P < 0.05, **P < 0.01, ***P < 0.001.

fractions of gel filtration. The presence of 3CLpro in the fractions, related to the protein complex with various molecular weights, could reflect the dynamic process in which 3CLpro gradually lost its solubility. Although most of the soluble 3CLpros were in the fractions with a molecular weight of around 60 kDa, which is the size of dimerized 3CLpro, we observed that 3CLpro migrated to the early-collected fractions with high molecular weight [11]. Importantly, the presence of 3CLpros in the early-collected fractions was increased for the cells treated with H_2O_2

(Fig. 4A–C). The result indicated the aggregation of 3CLpro was a dynamic process. In this process, 3CLpro could be sensitive to the alternation of oxidative activity in the intracellular environment. To visualize the structure and localization of 3CLpro aggregates in the cells, we used immune-staining to examine the cells transfected with 3CLpro-HA, observing that compared with untreated cells, 3CLpro formed more granular structures in the cells with H_2O_2 treatment (Fig. 4D and E).
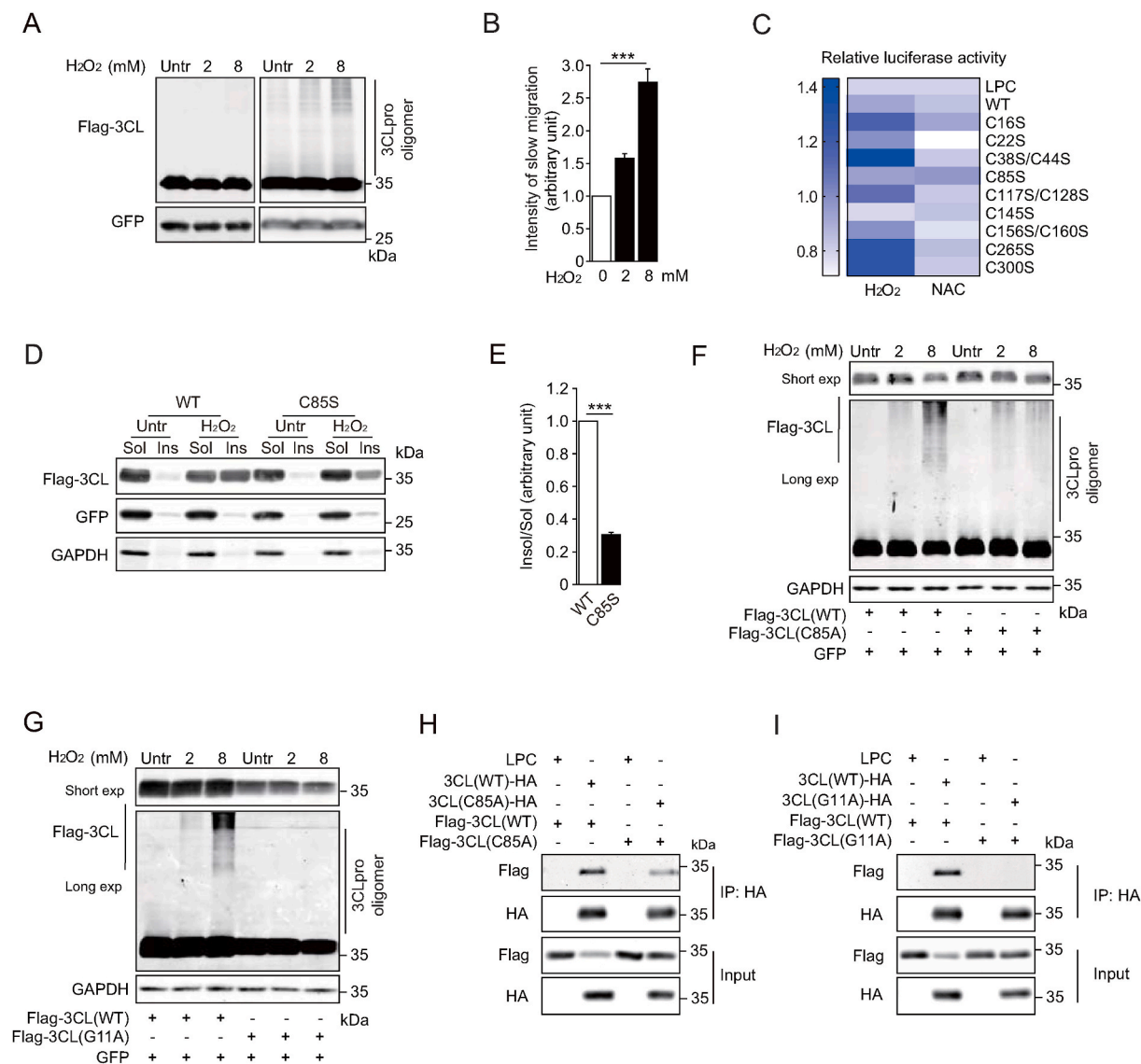
Fig. 5. C85 played a critical role in 3CLpro aggregation.
(A) HEK293T cells, transfected with Flag-3CL and GFP, were left untreated or treated with 2 mM or 8 mM H_2O_2 for 2 h. The cells were lysed in DISC IP buffer and cleared with centrifugation. The soluble fractions were subjected to WB with or without reducing agent, β-ME. The slow migrations of 3CLpro were quantified using Image Studio™ Lite Software, and the intensity of each slow migration of 3CLpro was normalized with related main 3CLpro bands (B). Note that H_2O_2 treatment increased the amount of slow migration of 3CLpro. (C) HEK293T cells were transfected with pRL-TK, Ub4-CS-Luci, and 3CLpro WT or various cysteine mutants. 24 h post-transfection, the cells were left untreated or treated with 2 mM H_2O_2 for 2 h or 16 mM NAC for 16 h, the cells were collected, and the lysates were subjected to Dual-Luciferase® Reporter (DLR™) Assay. Note that different from other 3CLpro mutants, the protease activity of 3CLpro C85S was less sensitive to H_2O_2 and NAC treatment. HEK293T cells, transfected with Flag-3CL WT and GFP or Flag-3CL C85S and GFP, were left untreated or treated with 2 mM H_2O_2 for 2 h. The soluble and insoluble samples were subjected to WB (D) and the ratios of Ins/Sol were analyzed using Image Studio™ Lite Software (E). HEK293T cells, transfected with Flag-3CL WT and GFP, or Flag-3CL C85A and GFP (F), or Flag-3CL G11A and GFP (G), were left untreated or treated with 2 mM or 8 mM H_2O_2 for 2 h. The cells were lysed in DISC IP buffer and cleared with centrifugation. The soluble fractions were subjected to WB with or without reducing agent, β-ME. HEK293T cells, transfected with LPC [35], Flag-3CL/3CL-HA WT, C85A (H), or G11A (I), 36 h post-transfection, the cells were subjected to immunoprecipitation assay with HA beads, and IP samples were subjected to WB analysis with indicated antibodies. The data represent one of three independent experiments with similar results; error bars represent the mean ± s.e.m. A two-tailed unpaired Student's t-test or one-way ANOVA with Bonferroni post-test correction was used to analyze the significance; *P < 0.05, **P < 0.01, ***P < 0.001.

2.5. The disulfide bonds formed at C85 are responsible for the insolubility of 3CLpro

One of the important consequences caused by H_2O_2 treatment is the formation of disulfide bonds from thiol groups of cysteines, which could change the protein structure, increase the protein complex size and even induce the insolubility of protein [26,29,30]. To obtain the evidence of the disulfide-bond formation, we analyzed the 3CLpro from cells left untreated or treated with H_2O_2 using the non-reducing SDS-PAGE and immunoblotting. The non-reducing condition could retain the disulfide bonds, and with SDS, various proteins could migrate in PAGE at the rate related to their molecular sizes [26]. The results showed that more 3CLpro migrated slowly after H_2O_2 treatment, indicating that H_2O_2 treatment could induce the disulfide-bond formation and thus increased molecular size (Fig. 5A and B).

To explore which cysteine residue in 3CLpro is essential for the aggregation, we mutated all cysteines of 3CLpro to serine and analyzed the amounts of soluble and insoluble fractions of these 3CLpro proteins with various mutations. In the untreated condition, the ratios of insoluble/soluble were comparable among various mutant 3CLpros (Figs. S3A, 5D, and 5E). After H_2O_2 treatment, the ratios were increased drastically for most of the mutant 3CLpros except for C85S and C22S (Figs. S3A, 5D, and 5E). To test whether these cysteine mutations affected the protease activity of 3CLpro, we employed 3CLpro activity reporter system to evaluate the protease activity of each mutant 3CLpro, which was left untreated or treated with H_2O_2 or NAC. The results showed that H_2O_2 increased and NAC decreased the protease activity of all mutant 3CLpros except C85S and C145S, the catalytic dead mutant [11] (Figs. 5C and S3B), consistent with the results for the distribution of insoluble and soluble fractions of various mutant 3CLpros.

To investigate the role of C85 in the formation of the 3CLpro-involved protein complex, we examined the H_2O_2-induced slow migration of 3CLpro with non-reducing WB. As expected, the C85S mutation decreased the H_2O_2-induced slow migration of 3CLpro compared with WT (Fig. 5F). Interestingly, the 3CLpro with G11A mutation, which impaired its capability to form the dimer, could also not form the protein complex with the high molecular weight, indicating the indispensable role of dimerization in the 3CLpro aggregation (Fig. 5G).

Since 3CLpro forms a dimer, which should be essential for the aggregation, we investigated whether C85A mutation would affect the 3CLpro dimerization. The results showed that C85A mutation could decrease the 3CLpro oligomerization (Fig. 5H), which is completely abolished by the G11A mutation (Fig. 5I), indicating that the C85 mediated the protein association of 3CLpro through a different way from G11 and the disulfide bonds were formed among 3CLpro proteins in the basal culture condition. Collectively, these data indicated that C85 could be a critical residue for the disulfide-bond formation of 3CLpro and the aggregation formation.

2.6. Oxidative stress facilitates the replication/transcription of SARS-CoV-2

3CLpro plays a critical role in the process of the viral polyprotein and the maturation of replicase complex, which is pivotal for viral replication/transcription. To confirm this critical role of 3CLpro, we expressed Rep-Luci (Fig. S1H) and pRL-TK with or without 3CLpro in HEK293T cells. The results showed that the expression of 3CLpro could significantly increase the activity of Rep-Luci, the replicon of SARS-CoV-2, indicating that 3CLpro encoded by SARS-CoV-2 was possibly inadequate for processing viral polyprotein, and additional 3CLpro could further promote the viral replication/transcription (Fig. 6A).

Since oxidative stress increased the activity of 3CLpro, which promoted the viral replication/transcription, we investigated whether oxidative stress could also promote the replication/transcription of viral replicon. We treated the cells transfected with Rep-Luci and pRL-TK with H_2O_2 and detected increased luciferase activity, indicating an increase

in replicon replication/transcription (Fig. 6B). Next, we explored whether the suppression of oxidative activity could inhibit viral replication/transcription. As predicted, NAC, a ROS scavenger, decreased the replication/transcription of the replicon (Fig. 6C).

To further explore the potential of antioxidants in the treatment of COVID-19, we used NAC to treat the cells, which were infected with SARS-CoV-2. The result showed that NAC (IC50 = 6.08 mM) inhibited the proliferation of SARS-CoV-2 significantly, indicating that the clinical application of antioxidants might benefit the therapy on patients infected with SARS-CoV-2 (Fig. 6D).

To further investigate the role of the disulfide formation in H_2O_2 induced viral replication/transcription, we introduced the mutation of 3CL C85S in the viral replicon, observing that the mutation decreased the subgenomic RNA amounts of replicon (Fig. 6E). The subgenomic RNA amounts of the 3CL C85S mutant replicon could not be increased by H_2O_2 treatment like WT replicon (Fig. 6F and G).

2.7. 3CLpro promotes the proximal oxidative activity by promoting cleavage of GPx1

Our aforementioned data supported that oxidative activity could promote the protease activity of 3CLpro. However, how the intracellular oxidative activity was increased was still obscure. The previous genome-wide viral protein interactome identified that GPx1 was associated with 3CLpro [31]. To confirm the relationship between 3CLpro and GPx1, we constructed the expression construct of GFP-GPx1 and co-expressed it with 3CLpro in 293T cells. The WB results showed that 3CLpro could promote the cleavage of GFP-GPx1 in a dosage-dependent manner (Fig. 7A), and the cleavage was 3CLpro protease activity and dimerization-dependent (Fig. 7B and C). Furthermore, we employed immunoprecipitation-mass spectrometry (IP-MS) to identify the cleavage site in GPx1 and found the cleavage happened between glutamate (28) and proline (29) (Fig. S4A), which were located on the GSHPx domain of GPx1, the only known function domain in GPx1 (Fig. S4B). The cleavage site identified by IP-MS differed from the consensus sequence of 3CLpro cleavage site, indicating that 3CLpro indirectly regulated the cleavage.

Since GPx1 plays an essential role in maintaining the cellular antioxidant capacity [32], we investigated whether the cleavage of 3CLpro on GPx1 could alter the intracellular oxidative activity. The overexpression of 3CLpro increased the overall oxidative activity intracellularly and led to cell death, which was attenuated by the overexpression of GPx1 (Fig. 7D, E, and 7F). To further investigate the relation of 3CLpro and oxidative activity, we stained the cells with H_2DCFDA and observed that the cellular localization of 3CLpro aggregate coincided with FITC puncta, indicating the 3CLpro altered the oxidative activity of its proximate area (Fig. 7G). Furthermore, the overexpression of GPx1 impaired the 3CLpro activity and consequently inhibited the replicon activity of SARS-CoV-2 (Fig. 7H and I).

3. Discussion

Due to the sequence conservation among various coronaviruses, well-defined structures, and essential roles in the process of the viral polyprotein, 3CLpro has been widely accepted to be a promising target for drug development. Therefore, a myriad of studies were carried out to develop drugs inhibiting the function of 3CLpro. Even though many drugs exhibited strong affinities to and inhibitory effects on the 3CLpro *in vitro*, their inhibitory effects were usually largely attenuated *in vivo* [2, 3]. This difference could be due to the difference between the exterior and interior cellular environment, which may even alter the structure of 3CLpro, while the molecular details were still unclear.

To study how the activity of 3CLpro is regulated *in vivo*, we constructed a 3CLpro activity reporter system, which could manifest the activity of 3CLpro quantitatively and dynamically (Fig. 1B). We screened various factors, including nutrient deprivations, metal ions,
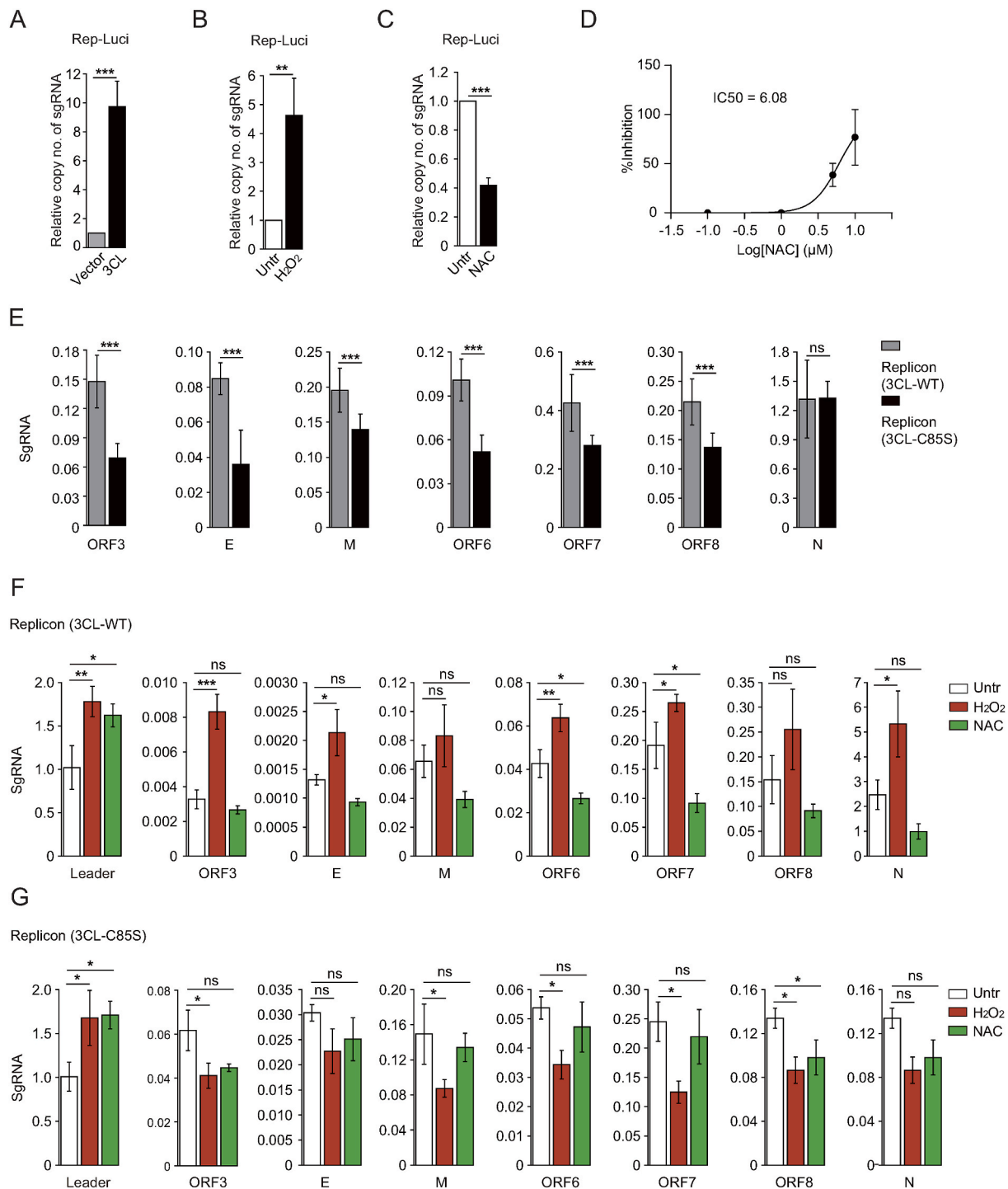
Fig. 6. Oxidative stress promoted the replication/transcription of SARS-CoV-2.
(A) HEK293T cells were transfected with Rep-Luci, pRL-TK, and vector or 3CL-HA. 72 h post-transfection, the cells were subjected to the Dual-Luciferase® Reporter (DLR™) Assay. Note that 3CLpro promoted the replication/transcription of the viral replicon. HEK293T cells, transfected with Rep-Luci and pRL-TK, were left untreated or treated with 0.5 mM H_2O_2 (B) or 10 mM NAC (C) for 2 days. The cells were subjected to the Dual-Luciferase® Reporter (DLR™) Assay. Note that H_2O_2 treatment increased the replicon activity, while NAC treatment decreased the replicon activity. (D) Vero E6 cells, infected with SARS-CoV-2 at MOI of 0.05 for 1 h, were cultured in a medium containing NAC with indicated concentrations. 48 h post-infection, the supernatants were harvested for qRT-PCR assay. The relation between the viral copies and NAC concentrations was analyzed using GraphPad Prism 6 software and presented in a dose-response curve. (E) HEK293T cells were transfected with GFP and Rep WT or Rep with 3CL C85S mutation. The cells were left untreated or treated with 0.5 mM H_2O_2 or 10 mM NAC for 2 days. The cells were harvested for qRT-PCR assay with primers for indicated subgenomic RNAs. The relative amount of each subgenomic RNA was analyzed as described in M&M. The comparison between the relative amounts of subgenomic RNAs of Rep WT and that of Rep with 3CL C85S mutation was presented. The comparisons among untreated, treated with H_2O_2, and treated with NAC for the relative amounts of subgenomic RNAs of Rep WT (F) or that of Rep with 3CL C85S mutation (G) were depicted. The data represent one of three independent experiments with similar results; error bars represent the mean ± s.e.m. A two-tailed unpaired Student's t-test or one-way ANOVA with Bonferroni post-test correction was used to analyze the significance; *P < 0.05, **P < 0.01, ***P < 0.001.
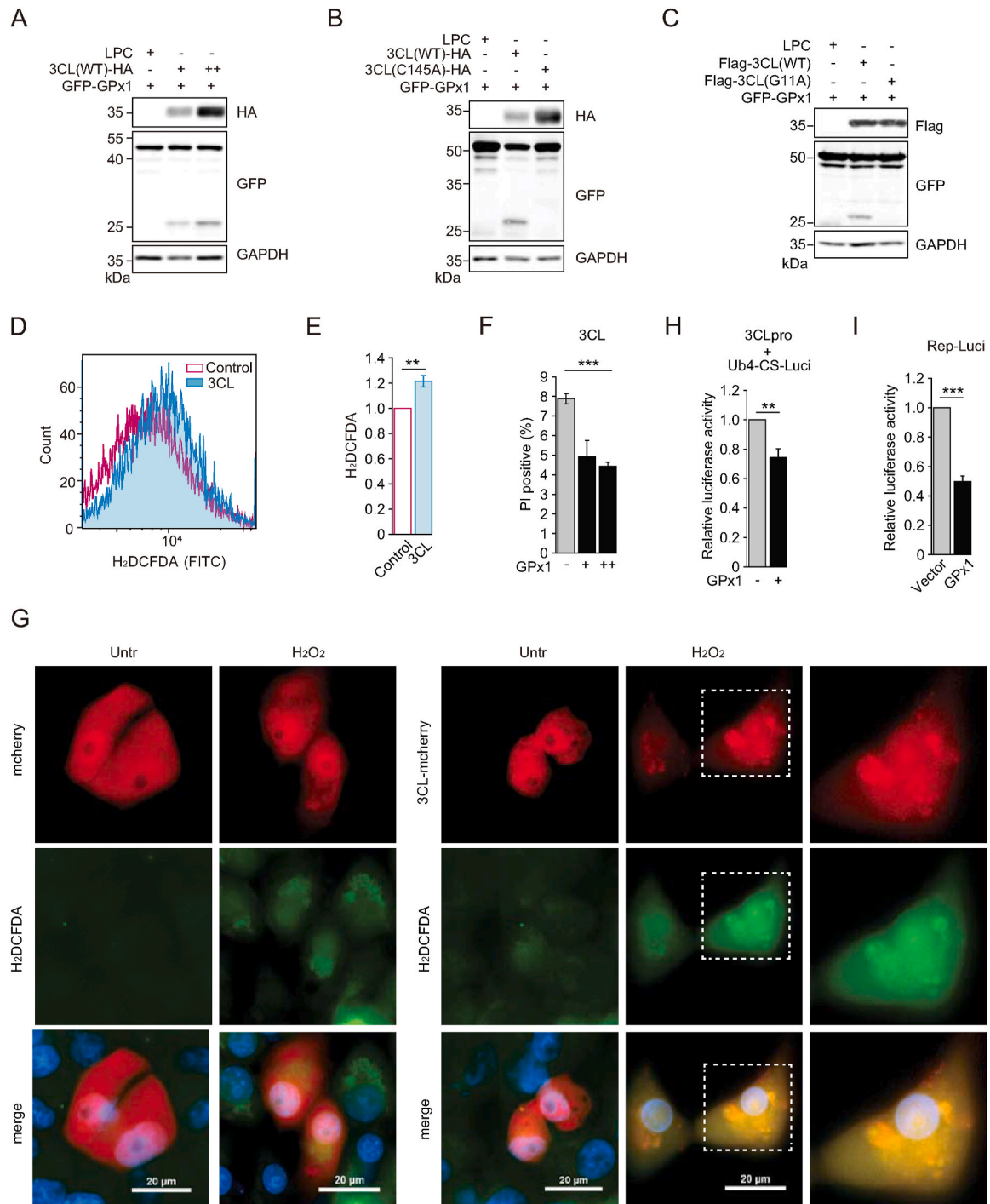
Fig. 7. 3CLpro impaired the intracellular antioxidant capacity through the cleavage of GPx1.
(A) HEK293T cells were transfected with GFP-GPx1 and vector, 0.5 μg or 1 μg of 3CL-HA plasmid. The cells were collected and subjected to WB analysis with indicated antibodies. Note that 3CLpro increased the amounts of cleaved GFP-GPx1 (the band with the molecular weight of 26 kDa) in a dose-dependent manner. Similar to (A), GFP-GPx1 was co-expressed with 3CLpro C145A (B) or G11A (C) in HEK293T cells. The cells were collected and subjected to WB analysis with indicated antibodies. Note that 3CLpro-mediated cleavage on GFP-GPx1 was diminished by the mutations of C145A or G11A. (D) and (E) HEK293T cells, transfected with 3CLpro, were stained with 5 μM H₂DCFDA (FITC) for 30 min and then were analyzed using CytoFLEX cytometry. (F) HEK293T cells, transfected with 3CLpro and GFP-GPx1, were collected and stained with propidium iodide (PI). The percentages of PI-positive cells were analyzed using CytoFLEX cytometry. (G) Vero E6 cells, transfected with 3CL-mCherry, were left untreated or treated with 2 mM H₂O₂ for 2 h. The cells were stained with 5 μM H₂DCFDA (FITC) for 30 min and then were observed under Nikon ECLIPSE Ti2. Note that 3CLpro colocalized with H₂DCFDA positive puncta. (H) HEK293T cells, transfected with a 3CLpro activity reporter system and GFP vector or GFP-GPx1, were subjected to Dual-Luciferase® Reporter (DLR™) Assay. (I) HEK293T cells, transfected with Rep-Luci and RL-TK, and GFP vector or GFP-GPx1, were subjected to Dual-Luciferase® Reporter (DLR™) Assay. The data represent one of three independent experiments with similar results; error bars represent the mean ± s.e.m. A two-tailed unpaired Student's t-test or one-way ANOVA with Bonferroni post-test correction was used to analyze the significance; *P < 0.05, **P < 0.01, ***P < 0.001.

metabolites, and oxidative stress inducers, for their impacts on the activity of 3CLpro (Fig. 2 and S2). Oxidative stress, which is known as a factor against viral infection, promoted the activity of 3CLpro (Fig. 2E, G, and 2I). We also found that the H_2O_2 treatment could increase the activity of SARS-CoV-2 replicon, and ROS scavengers could suppress the replication of the live virus (Fig. 6B–D). These data indicated that oxidative stress could benefit viral replication, possibly by increasing the activity of 3CLpro.

Containing physiological concentration of salt, neutral pH, and mild detergent, DISC IP buffer is widely used to extract the proteins from mammalian cells. Using DISC IP buffer, we extracted less 3CLpro from H_2O_2-treated cells compared with untreated cells. The decreased amount of 3CLpro proteins was contradictory to the finding of increased 3CLpro activity upon H_2O_2-treatment. Using RIPA buffer, we identified an increased DISC IP buffer-insoluble 3CLpro in H_2O_2-treated cells. The identification of insoluble 3CLpro provided the clue to explore the cause of increased 3CLpro activity.

Increasing evidence showed that aggregation could promote protein functions. MAVS, a key component of RIG-1-MAVS-IRF3 pathway, forms prion-like aggregates to activate the IRF3 [33]. pGAM5 short form, which is insoluble in the lysis buffer containing 1% Triton-X-100 like DISC IP buffer, plays a critical role in necrosis execution [34]. These findings lead us to hypothesize that insoluble 3CLpro is likely an intracellular functional form.

To explore the molecular details of insoluble 3CLpro, we firstly focused on the impact of oxidative stress. Using gel filtration, we identified 3CLpro's intermediate conditions from soluble to insoluble (Fig. 4A and B). H_2O_2-treatment significantly increased the amount of 3CLpro in the intermediate states, in which molecular weights of 3CLpro involved protein complexes were higher than that of 3CLpro dimer. Thiol is one of the most sensitive groups to oxidative stress, and the formation of disulfide bonds could alter the protein structure and even solubility. Therefore, we screened 3CLpro with the various cysteine mutations for their impact on the insolubility and identified that C85S mutation drastically decreased the amount of H_2O_2-induced insoluble 3CLpro, indicating that C85 could be the key residue mediating the formation of disulfide bond among 3CLpro dimers.

Thus far, seven human coronaviruses, including SARS-CoV, SARS-CoV-2, OC43, HKU1, MERS-CoV, 229E, and NL63, were reported [4,5]. The analysis of 3CLpro amino acid sequences of various coronaviruses depicted that besides C16, C38, and C145, which are key residues for the substrate interaction or the catalytic activity [11], C85 is the most conserved cysteine (Fig. S6A), suggesting that oxidative-stress induced activation of 3CLpro could be a conservative mechanism of coronavirus.

3CLpro performs its protease activity as a dimer. Unlike the other cysteines, which are mostly located inside the molecule or on the interface for the dimerization, C85 is located on the periphery of 3CLpro (Figs. S3C and S3D). Its thiol group forms hydrogen bonds with H_2O, indicating that it plays an essential role in the solubility maintenance of 3CLpro (Fig. S3E).

We predicted that upon the H_2O_2 treatment, the C85S of various adjacent 3CLpro dimers were covalently linked with each other by disulfide bonds, which gradually increased the protein complex size with more dimers being involved in, reduced the C85 interaction with H_2O, and eventually likely led to the insolubility of the protein complex (Fig. S3F). Although the solubility was altered, the core structures of 3CLpro for protease activity should not be changed, and thus the enzymatic activity retained. In the dimer of 3CLpro, one protomer was active, and the other functions as a regulator (Fig. S3F) [11]. In the oligomer or polymer linked by the disulfide bond, one promoter could be in an active form and function as a regulator simultaneously. This oligomer or polymer structure could also establish a separate space for the catalytic reaction, thus avoiding the interference of other host proteins.

We found that the expression of replicon or 3CLpro could increase the overall intracellular oxidative activity (Fig. 2K, L, 7D, and 7E),

indicating that viral replicon could impact the cellular redox regulatory system. GPx1, a member of GPx family that mainly catalyzes the reduction of hydroperoxides and hydrogen peroxide (H_2O_2) to protect cells from oxidative damage, was reported to be the interaction partner of 3CLpro [31]. Here, we found that GPx1 could be cleaved at its N-terminus, which was regulated by 3CLpro, and the cleavage sites are conserved across GPx1s of various species (Fig. S5A). By this strategy, the SARS-CoV-2 could build an oxidative environment for 3CLpro aggregation and further activity promotion, benefiting viral replication in cells (Fig. S7).

In summary, we reported here that 3CLpro performed its protease activity in two different forms intracellularly. Oxidative stress could induce the formation of DISC IP buffer-insoluble 3CLpro, which accounted for the increased proteolytic activity. Through inhibiting the function of the GPx1 and attenuating intracellular antioxidative capacity, 3CLpro forms a more active form and drives the viral replication in the cells. Our study provided an important clue to understanding the regulation of intracellular 3CLpro activity, which could help fill the knowledge gap in the different behaviors of 3CLpro *in vitro/in vivo*.

4. Materials and methods

4.1. Cell lines and culture

HEK293T cells were cultured in Dulbecco's modified Eagle's medium (DMEM) (Thermo Fisher Scientific, C11960500), supplemented with 10% fetal bovine serum (FBS) (Thermo Fisher Scientific, A3160801), 100 unit/mL penicillin, 100 μg/mL streptomycin (Thermo Fisher Scientific, 15140–122), and 2 mM L-Glutamine (Thermo Fisher Scientific, 25030–081) at 37 °C with 5% CO_2.

DMEM basal medium (Shanghai BasalMedia Technologies Co., LTD., X014C) contains 40 μM phenol red, 25 mM HEPES, 10 mM sodium pyruvate, 44 mM sodium bicarbonate, and multiple vitamins. For nutrient deprivation assay, the other nutrients for regular DMEM were added in basal medium except for the one intended to be deprived, including EAA (Shanghai BasalMedia Technologies Co., LTD., S230JV), NEAA (Thermo Fisher Scientific, 11140–050), Glucose (Sangon Biotech, A100188-0500).

4.2. Reagents and antibodies

The following antibodies were used: polyclonal rabbit anti-GFP antibody (Proteintech, 50430-2-AP, 1:1000 for WB), mouse anti-HA antibody (Biolegend, 901515, 1:1000 for WB, 1:500 for IF), mouse anti-FLAG antibody (Sigma-Aldrich, F1804, 1:2000 for WB, 1:500 for IF), GAPDH polyclonal rabbit antibody (Proteintech, 10494-1-AP), GAPDH monoclonal mouse antibody (Proteintech, 60004-1-Ig), Anti-Tubulin antibody produced in rabbit (Sigma-Aldrich, T3526), Alpha tubulin monoclonal mouse antibody (Proteintech, 66031-1-Ig), goat anti-mouse antibody (LI-COR, 926–32211, 1:10,000 for WB), goat anti-rabbit antibody (LI-COR, 926–68070, 1:10,000 for WB), Alexa Fluor™ 594 goat anti-mouse IgG (H + L) (Thermo Fisher Scientific, A11005, 1:1000 for IF), Alexa Fluor™ 488 goat anti-rabbit IgG (H + L) (Thermo Fisher Scientific, A11008, 1:1000 for IF).

The following reagents were used: H_2O_2 (Sigma-Aldrich, 7722-84-1), L-ascorbic acid (Sangon Biotech, A100143-0100), NAC (Sigma-Aldrich, A9165), L-(+)-lactic acid (Rhawn, R005612), Tris (Sangon Biotech, 77-86-1), $MgCl_2$ (Sangon Biotech, 7791-18-6), $CaCl_2$ (Sigma-Aldrich, 10043-52-4), $MnCl_2$ (Sigma-Aldrich, 7773-01-5), MG132 (Sigma-Aldrich, C2211), Bafilomycin-A1 (Sigma-Aldrich, 88899-55-2), Goat serum (Sangon Biotech, E510009), 4′,6-diamidino-2-phenylindole dihydrochloride (DAPI) (Sigma D9542, used at 1 μg/mL), 4% paraformaldehyde (YEASON, 36314ES76), Triton-X-100 (Sigma-Aldrich, 9002-93-1), HIS-Select® Nickel Magnetic Agarose Beads (Sigma-Aldrich, H9914-1 ML), Isopropanol (Sangon Biotech, 67-63-0), TRIzol™ Reagent (Invitrogen, AM9738), propidium iodide (PI) (YEASON, 25535-

16-4). SYBR Premix Ex Taq (TAKARA, RR420A), Dual-Glo® Luciferase reporter assay system (Promega, E1960), and Revert Aid First Strand cDNA Synthesis Kit (Thermo Fisher Scientific, K1622), Hieff TransTM Liposomal Transfection Reagent (YEASEN, 40802 ES03), Cell Line NucleofectorTM Kit V (LONZA), Pierce™ BCA Protein Assay Kit (Thermo Fisher Scientific, 23227), Fluoromount (Sigma-Aldrich, F4680), NEBuilder HiFi DNA Assembly Master Mix (NEB, E2621L), Hoechst 33342 (Biosharp BL803A).

4.3. Plasmid construction

The coding sequence of 3CLpro was amplified by PCR with the primers fused with the sequence of HA or Flag tag. The PCR fragments were inserted between *Hind*III and *Xho*I sites in LPC vector [35]. The 3CLpro mutant of G11A, H41A, C145S, C145A, M162A, H163A, C16S, C22S, C38/44S, C85S, C85A, C117/128S, C156/160S, C265S, or C300S was generated via site-directed mutagenesis [35]. The sequences of primers are listed in Table 1. The ubiquitin-luciferase reporter (Ub-Luci) was generated via fusion of the firefly luciferase (FL) to the *Homo sapiens* ubiquitin (Ub). For the Ub4-Luci containing repeats of Ubs, the strategy of NEBuilder HiFi DNA Assembly Master Mix (NEB, E2621L) was used to link Ubs and then fused the sequences of multiple Ubs with FL. The sequences of primers are listed in Table 2. The 3CLpro consensus cleavage sequence was synthesized and inserted to the reserved *Hind*III site between Ub4 and FL to generate Ub4-CS-FL, and the 3CLpro cleavage sequences in ORF1ab were also inserted separately into Ub4-FL as described above. The sequences of primers are listed in Table 2. All the constructs were validated by Sanger DNA sequencing (Tsingke Biotechnology Co., Ltd. Beijing). The details of the construction of SARS-CoV-2 replicon and the replicon expressing luciferase were described previously [27].

Table 1
Primers for mutagenesis.

Names	Primer sequences (5′-3′)
H41A f	TGCCCGCGTGCCGTTATCTGCACCAGCG
H41A r	GCAGATAACGGCACGCGGGCAGTAAACCAC
G11A f	TTTCCGAGCGCCAAAGTTGAAGGTTGCAT
G11A r	CAACTTTGGCGCTCGGAAACGCCATCTTA
C145S f	CGGTAGCTCCGGCAGCGTGGGTTTCAAC
C145S r	CGCTGCCGGAGCTACCGTTCAGAAAGCTAC
C145A f	CGGTAGCGCAGGCAGCGTGGGTTTCAAC
C145A r	CGCTGCCTGCGCTACCGTTCAGAAAGCTAC
M162A f	GCTTTTGCTATGCGCACCACATGGAGCTGCCG
M162A r	CCATGTGGTGCGCATAGCAAAAGCTAACGCAATCG
H163A f	GCTATATGGCCCACATGGAGCTGCCGACCG
H163A r	GCTCCATGTGGGCCATATAGCAAAAGCTAACGC
C16SC22S f	TGCACCATGGAACCTTCAACTTTGCCGCTCGG
C16SC22S r	AGTTACCTCCGGCACCACCACCCTGAACG
C38SC44S f	GTTATCTCCACCAGCGAGGACATGCTGAACCCG
C38SC44S r	GTGACGCGGGGAGTAAACCACATCGTCCAGCC
C85S f	AAGCTGAAAGTTGACACCGCGAACCCGAAAACCC
C85S r	CAGCACGGAGTTCTGCATGCTGTGACCGAT
C85A f	AGAACGCCGTGCTGAAGCTGAAAGTTGACACCGC
C85A r	CACGGCGTTCTGCATGCTGTGACCGATAACACGC
C117SC128S f	CGAGCGGTGTTTATCAATcCGCGATGCGTCCG
C117SC128S r	GGCTGCCGTTGTAGGACGCCAGAACGC
C156SC160S f	CTTTTCCTATATGCCACCATGGAGCTGCCGACC
C156SC160S r	CTAACGGAATCGTAGTCAATGTTGAAACCCACGCTGCC
C265S f	GCCTGAAAGAACTGCTGCAGAACGGCATGAACGG
C265S r	TCGCGGACATATCCAGCACCGCAATACCGG
C300S f	GGTTCGTCAGTCCAGCGGTGTGACCTTTCAATAA
C300S r	ACATCAAACGGGGTGAATTCGTCCTCCAGCAGCG
Rep-3CL C85S f	CATTCTATGCAAAATAGTGTACTTAAGCTTAAG
Rep-3CL C85S r	CTTAAGCTTAAGTACACTATTTTGCATAGAATG
Rep-7994 f	GTGTCTGATGTTGGTGATAGTGCGG
Rep-11758 r	GGGTGGGAGTAGTCCCTGTG
Rep-8320 f	CCGTGACCTTGGTGCTTGTATTG
Rep-10802 r	CAGTTTGAGCAGAAAGAGGTCCTAG
GPx1 U47C f	CCTCTGCGGCACCACGGTCCGGGACTACA
GPx1 U47C r	GGTGCCGCAGAGGGACGCCACATTCTCGATAAGTAGTAC

Table 2
Primers for the 3CLpro activity reporter system.

Names	Primer sequences (5′-3′)
3CL f	CCGAAGCTTACCATGAGCGGTTTCCGTAAGATGGC
3CL r	CCCTCGAGTTGAAAGGTCACACCGCTGC
CS f	AGCTTAATGTGGCAACTTTACAGAGTGCTAATGCTACTA
CS r	AGCTTAGTAGCATTAGCACTCTGTAAAGTTGCCACATTA
CS(Q→N) f	GGCAACTTTAAACAGTGCTAATGCTACTAAGCTTGGAAGAC
CS(Q→N) r	GCATTAGCACTGTTTAAAGTTGCCACATTAAGCTTACTAGTC
CS(LQS→AAG) f	AGCTTAATGTGGCAACTGCCGCGGGAGCTAATGCTACTA
CS(LQS→AAG) r	AGCTTAGTAGCATTAGCTCCCGCGGCAGTTGCCACATTA
NSP1/2 f	AGCTTCGTGAGCTTAACGGAGGGGCATACACTCGCTATA
NSP1/2 r	AGCTTATAGCGAGTGTATGCCCCTCCGTTAAGCTCACGA
NSP2/3 f	AGCTTTCACACTCAAAGGCGGTGCACCAACAAAGGTTA
NSP2/3 r	AGCTTAACCTTTGTTGGTGCACCGCCTTTGAGTGTGAAA
NSP3/4 f	AGCTTATAGCACTTAAGGGTGGTAAAATTGTTAATAATA
NSP3/4 r	AGCTTATTATTAACAATTTTACCACCCTTAAGTGCTATA
NSP4/5 f	AGCTTACCTCAGCTGTTTTGCAGAGTGGTTTTAGAAAAA
NSP4/5 r	AGCTTTTTTCTAAAACCACTCTGCAAAACAGCTGAGGTA
NSP5/6 f	AGCTTTCAGGTGTTACTTTCCAAAGTGCAGTGAAAAGAA
NSP5/6 r	AGCTTTCTTTTCACTGCACTTTGGAAAGTAACACCTGAA
NSP6/7 f	AGCTTAAAGTAGCCACTGTACAGTCTAAAATGTCAGATA
NSP6/7 r	AGCTTATCTGACATTTTAGACTGTACAGTGGCTACTTTA
NSP7/8 f	AGCTTAACAGGGCAACCTTACAAGCTATAGCCTCAGAGA
NSP7/8 r	AGCTTCTCTGAGGCTATAGCTTGTAAGGTTGCCCTGTTA
NSP8/9 f	AGCTTTCTGCTGTCAAATTACAGAATAATGAGCTTAGTA
NSP8/9 r	AGCTTACTAAGCTCATTATTCTGTAATTTGACAGCAGAA
NSP9/10 f	AGCTTGCCACAGTACGTCTACAAGCTGGTAATGCAACAA
NSP9/10 r	AGCTTTGTTGCATTACCAGCTTGTAGACGTACTGTGGCA
NSP10/11 f	AGCTTCGCGAACCCATGCTTCAGTCAGCTGATGCACAAA
NSP10/11 r	AGCTTTTGTGCATCAGCTGACTGAAGCATGGGTTCGCGA
NSP12/13 f	AGCTTCCGCATACAGTCTTACAGGCTGTTGGGGCTTGTA
NSP12/13 r	AGCTTACAAGCCCCAACAGCCTGTAAGACTGTATGCGGA
Nsp13/14 f	AGCTTAATGTGGCAACTTTACAAGCTGAAAATGTAACAA
Nsp13/14 r	AGCTTTGTTACATTTTCAGCTTGTAAAGTTGCCACATTA
NSP14/15 f	AGCTTACTTTTACAAGACTTCAGAGTTTAGAAAATGTGA
NSP14/15 r	AGCTTCACATTTTCTAAACTCTGAAGTCTTGTAAAAGTA
NSP15/16 f	AGCTTTTTTACCCAAAATTACAATCTAGTCAAGCGTGGA
NSP15/16 r	AGCTTCCACGCTTGACTAGATTGTAATTTTGGGTAAAAA
UB f	CCGTCTCCATGCAGATCTTCGTGAAGACTCTG
UB r	CCGTCTCTGCATGGTGAATCTAGTCACCACACC
Nhe1-UB f	CTAGCTAGCACCATGCAGATCTTCGTGAAGACTCTG
Luci r	CAGGGCGTATCTCTTCATAGCC

4.4. Dual-luciferase reporter assay

One day before transfection, HEK293T cells (1×10^5) were plated in 24-well plates. For each assay, LPC (0.5 µg), which was used as vector control, LPC-3CL-HA or its mutants (0.5 µg), Ub4-CS-FL (0.1 µg) or Ub4-FL (0.1 µg), pRL-TK (0.2 µg) were transfected into the cells using Hieff TransTM Liposomal Transfection Reagent. 24 h post-transfection, the transfected cells were left untreated, treated with indicated reagents, or cultured in media deprived of indicated nutrients. After treatment, the cells were lysed in passive lysis buffer (PLB, Promega, E1941). The activities of firefly and renilla luciferase were measured using Dual-Glo® Luciferase Assay System to determine the relative luciferase activities.

4.5. Subgenomic RNA analysis

HEK293T cells were transfected with replicon or replicon with 3CL C85S mutation and pEGFP-C1. The transfected cells were left untreated or treated with 0.5 mM H_2O_2 or 10 mM NAC for 2 days. RNA from these HEK293T cells was isolated by TRIzol™ Reagent (Thermo Fisher Scientific). 5 µg of total RNA was subjected to reverse-transcription with oligo (dT) primer to obtain cDNA using Revert Aid First Strand cDNA Synthesis Kit. For qPCR, the cDNA was diluted at the ratio of 1:3, and 1 µL of each sample was used for each assay containing SYBR Premix Ex Taq. The primers for the subgenomic RNAs of replicon and GFP were listed in Table 3. The qPCR condition was 40 cycles of 5 s at 95 °C and 3 s at 60 °C. The levels of subgenomic RNAs were normalized with GFP, which was used as an internal control [27].

Table 3
Primers for qRT-PCR.

Names	Primer sequences (5′- 3′)
Leader f	CCTTCCCAGGTAACAAACCAACC
Leader r	CTCTCCATCTTACCTTTCGGTCAC
ORF3 r	GTGCAACGCCAACAATAAGCCATC
E r	GACTCACGTTAACAATATTGCAGCAG
M r	GCATAGGCAAATTGTAGAAGACAAATCC
ORF6 r	GTCAACGAGATGAAACATCTGTTGTCAC
ORF7 r	GAGTGCTAAAGCAAGTCAGTGC
ORF8 r	GGTGCTGATTTTCTAGCTCCTACTC
N r	CAGTATTATTGGGTAAACCTTGGGGC
GFP f	TACGGCAAGCTGACCCTGAAG
GFP r	TGAAGCACTGCACGCCGTAGG

4.6. Antiviral activity assays

Vero E6 cells were seeded at 1×10^5 cells per well in 24-well plates. Cells were allowed to recover for 24 h and then infected with SARS-CoV-2 at an MOI of 0.05 for 1 h at 37 °C. Then the viral inoculum was removed, and the cells were washed two times with pre-warmed phosphate-buffered saline (PBS). A medium containing various dilutions of NAC or DMSO was added. 48 h post-infection, supernatants were harvested for qRT-PCR analysis. The dose-response curves for viral RNA copies versus the drug concentrations were plotted using GraphPad Prism 6 software [36].

4.7. Cellular fractionation

For the separation of soluble and insoluble components, cells were lysed in DISC IP buffer (50 mM Tris-HCl, pH 7.5, 1% Triton-X-100, 10% glycerol, and 150 mM NaCl), supplemented with 1 mM PMSF, 1 × protease inhibitor cocktail, and 1 mM Na$_3$VO$_4$. The lysates were clarified with centrifugation at 12,000×g for 20 min at 4 °C. The supernatant was collected as a soluble component, while the pellet was washed once with DISC IP buffer and dissolved in RIPA buffer (50 mM Tris-HCl, pH 8.0, 0.5% sodium deoxycholate, 1% sodium dodecyl sulfate (SDS), 1% Triton-X-100, 150 mM NaCl) with sonication [26].

4.8. Western blotting

All lysates were quantified with BCA protein assay reagent (Thermo Fisher Scientific, 23227) and run on the 11.5% sodium dodecyl sulfate-polyacrylamide gel (SDS-PAGE) under the condition of 60 v. After that, proteins were transferred to nitrocellulose membranes at 120 v for 90 min. The membranes were blocked with PBS containing 5% non-fat milk and 0.05% Tween 20 (PBST) (WB blocking buffer) for 1 h at room temperature. Primary antibodies (1; 1000) against Tubulin, GAPDH, HA, GFP, FLAG were incubated at 4 °C overnight. The membranes were washed four times with PBST and then incubated in WB blocking buffer with the goat anti-rabbit or goat anti-mouse secondary antibody (1:10,000) for 1 h at room temperature. The membranes were washed 5 times again with PBST and finally imaged by an Odyssey Imager (LI-COR), and all the bands were normalized with GAPDH or Tubulin bands which served as the internal reference [26].

4.9. Immunofluorescence

HeLa or Vero E6 cells were seeded on glass coverslips in 24-well dishes and transfected with indicated plasmids. 24 h post-transfection, the cells were left untreated or treated with H$_2$O$_2$. After treatment, the cells were fixed in 4% paraformaldehyde (PFA) at room temperature for 20 min and washed twice with PBST. The cells were permeabilized with PBS containing 0.1% Triton-X-100 for 10 min. After being washed with PBS and PBST (PBS with 0.5% Tween 20), the cells were blocked with PBST containing 5% goat serum (IF blocking buffer) for 1 h at room temperature and then washed with PBST. Samples were incubated with IF blocking buffer containing mouse anti-HA antibodies or rabbit anti-HA antibodies (1:500) at 4 °C overnight and were washed four times with PBST the following day. Next, the cells were probed with secondary antibodies in IF blocking buffer for 1 h at room temperature. After being washed three times with PBST and one time with PBS, the cells were incubated with 1 μg/mL DAPI in PBS for 5 min and then washed twice in PBS. The slides were then fixed with Fluoromount (Sigma-Aldrich, F4680), imaged with Zeiss Confocal LSM800 Microscope [26].

For H2DCFDA staining, the cells were plated in a glass-bottom cell culture dish (NEST, 801002). After one-day recovery, the cells were transfected with 3CL-mcherry or mcherry. 24 h post-transfection, the cells were left untreated or treated with H$_2$O$_2$ and then incubated with CM-H2DCFDA at 10 μM and 1 μg/mL Hoechst 33342 for 30 min in the dark. After being washed twice with PBS, the cells were imaged with the confocal microscope (Nikon, ECLIPSE Ti2E), and analyzed by the NIS software [37].

4.10. Measurement of cell death

For cell death assessment, cells, including the detached ones and the resuspended ones by trypsinization, were collected and precipitated with centrifugation at 1000×g for 5 min. The cell pellets were resuspended in PBS supplemented with 10% FBS and propidium iodide (PI) at 1 μg/mL. Cell death was determined by counting PE5.5 positive events using a CytoFLEX (Beckman) [35].

4.11. Measurement of intracellular ROS

Cells were incubated with CM-H$_2$DCFDA at 10 μM for 30 min in the dark. Then the cells, including the detached ones and the resuspended ones by trypsinization, were collected and precipitated with centrifugation at 1000×g for 5 min. The cell pellets were resuspended in PBS containing 10% FBS. The intracellular ROS level of cells was determined by measuring the intensity of FITC using a CytoFLEX [37].

4.12. Gel filtration chromatography

The gel filtration chromatography was performed according to the strategy described previously [26]. In brief, cells were seeded on 10-cm dishes and transfected with LPC-3CL-HA and GFP. 24 h post-transfection, the transfected cells were left untreated or treated with H$_2$O$_2$. After treatment, the cells were lysed in DISC IP buffer, and the lysates were clarified with centrifugation at 12,000×g for 20 min at 4 °C. The supernatant was collected as a soluble component, passed through a 0.45 μm filter, and further fractionated by gel filtration chromatography using AKTA purifier with Superdex 200 10/300 GL. 0.5 mL of eluted samples for each fraction was collected and further analyzed by western blotting.

4.13. Immunoprecipitation

The immunoprecipitation was performed according to the strategy described previously [26]. Briefly, 293T cells were transfected with Flag- or HA-tagged 3CL and other indicated plasmids. 24 h post-transfection, the cells were lysed in DISC IP buffer, and the lysates were clarified with centrifugation at 12,000×g for 20 min at 4 °C. For anti-Flag or HA immunoprecipitation, the supernatants were incubated with pre-equilibrated Flag or HA agarose at 4 °C overnight. The complexes were centrifuged at 6000×g for 2 min at 4 °C, and washed with DISC washing buffer to remove the nonspecific binding proteins. The proteins of interest were eluted with pH 3.5 acidic buffer, and the eluted samples were neutralized with 1/10 volume of neutralization buffer (0.5 M Tris-HCl, pH 7.4, 1.5 M NaCl). Finally, the eluted samples were further analyzed by western blotting.

4.14. Statistics

All the experiments were performed at least three times. The data analyses were finished using Origin 8.0, Prism GraphPad, SPSS, or Excel. Statistical analyses were performed using an unpaired, two-tailed Student's t-test or one-way ANOVA with Bonferroni post-test correction. Results were considered significant when *P*-value was less than 0.05.

4.15. Image processing

Images were processed in Adobe Photoshop and Illustrator to enhance the brightness and contrast. The densitometry of immunoblot bands was determined using Image Studio™ Lite Software (LI-COR Biosciences) or ImageJ software.

Authors' contributions

JAP and XXP conceived the ideas and designed the experiments. XXP and JAP wrote the paper. All authors performed experiments or data analysis. All authors read and approved the final manuscript.

Availability of data and materials

All data generated or analyzed during this study are included in this published article and its supplementary information files.

Declaration of competing interest

The authors declare that they have no conflict of interest.

Appendix A. Supplementary data

Supplementary data to this article can be found online at https://doi.org/10.1016/j.redox.2021.102199.

References

[1] W.D. Jang, S. Jeon, S. Kim, S.Y. Lee, Drugs repurposed for COVID-19 by virtual screening of 6,218 drugs and cell-based assay, Proc. Natl. Acad. Sci. U. S. A. (2021) 118.

[2] Z. Jin, X. Du, Y. Xu, et al., Structure of M(pro) from SARS-CoV-2 and discovery of its inhibitors, Nature 582 (2020) 289–293.

[3] Z. Jin, Y. Zhao, Y. Sun, et al., Structural basis for the inhibition of SARS-CoV-2 main protease by antineoplastic drug carmofur, Nat. Struct. Mol. Biol. 27 (2020) 529–532.

[4] P. Zhou, X.L. Yang, X.G. Wang, et al., A pneumonia outbreak associated with a new coronavirus of probable bat origin, Nature 579 (2020) 270–273.

[5] Y. Chen, Q. Liu, D. Guo, Emerging coronaviruses: genome structure, replication, and pathogenesis, J. Med. Virol. 92 (2020), 2249-2249.

[6] J. Pan, X. Peng, Y. Gao, et al., Genome-wide analysis of protein-protein interactions and involvement of viral proteins in SARS-CoV replication, PLoS One 3 (2008) e3299.

[7] S. Hussain, J. Pan, Y. Chen, et al., Identification of novel subgenomic RNAs and noncanonical transcription initiation signals of severe acute respiratory syndrome coronavirus, J. Virol. 79 (2005) 5288–5295.

[8] P. V'kovski, A. Kratzel, S. Steiner, H. Stalder, V. Thiel, Coronavirus biology and replication: implications for SARS-CoV-2, Nat. Rev. Microbiol. 19 (2021) 155–170.

[9] E. de Wit, N. van Doremalen, D. Falzarano, V.J. Munster, SARS and MERS: recent insights into emerging coronaviruses, Nat. Rev. Microbiol. 14 (2016) 523–534.

[10] Y. Liu, C. Liang, L. Xin, et al., The development of Coronavirus 3C-Like protease (3CL(pro)) inhibitors from 2010 to 2020, Eur. J. Med. Chem. 206 (2020), 112711.

[11] H. Yang, M. Yang, Y. Ding, et al., The crystal structures of severe acute respiratory syndrome virus main protease and its complex with an inhibitor, Proc. Natl. Acad. Sci. U. S. A. 100 (2003) 13190–13195.

[12] V. Mody, J. Ho, S. Wills, et al., Identification of 3-chymotrypsin like protease (3CLPro) inhibitors as potential anti-SARS-CoV-2 agents, Commun Biol 4 (2021) 93.

[13] M. Tahir Ul Qamar, S.M. Alqahtani, M.A. Alamri, L.L. Chen, Structural basis of SARS-CoV-2 3CL(pro) and anti-COVID-19 drug discovery from medicinal plants, J Pharm Anal 10 (2020) 313–319.

[14] R. Alexpandi, J.F. De Mesquita, S.K. Pandian, A.V. Ravi, Quinolines-Based SARS-CoV-2 3CLpro and RdRp inhibitors and spike-RBD-ACE2 inhibitor for drug-repurposing against COVID-19: an in silico analysis, Front. Microbiol. 11 (2020) 1796.

[15] M. Sisay, 3CL(pro) inhibitors as a potential therapeutic option for COVID-19: available evidence and ongoing clinical trials, Pharmacol. Res. 156 (2020), 104779.

[16] A.D. Stephens, M. Zacharopoulou, G.S. Kaminski Schierle, The cellular environment affects monomeric alpha-synuclein structure, Trends Biochem. Sci. 44 (2019) 453–466.

[17] B.L. Strehler, Bioluminescence assay: principles and practice, Methods Biochem. Anal. 16 (1968) 99–181.

[18] G.D. Luker, C.M. Pica, J. Song, K.E. Luker, D. Piwnica-Worms, Imaging 26S proteasome activity and inhibition in living mice, Nat. Med. 9 (2003) 969–973.

[19] S. Chen, L.L. Chen, H.B. Luo, et al., Enzymatic activity characterization of SARS coronavirus 3C-like protease by fluorescence resonance energy transfer technique, Acta Pharmacol. Sin. 26 (2005) 99–106.

[20] S. Chen, T. Hu, J. Zhang, et al., Mutation of Gly-11 on the dimer interface results in the complete crystallographic dimer dissociation of severe acute respiratory syndrome coronavirus 3C-like protease: crystal structure with molecular dynamics simulations, J. Biol. Chem. 283 (2008) 554–564.

[21] D. Shi, R. Yan, L. Lv, et al., The serum metabolome of COVID-19 patients is distinctive and predictive, Metabolism 118 (2021), 154739.

[22] J. Michl, K.C. Park, P. Swietach, Evidence-based guidelines for controlling pH in mammalian live-cell culture systems, Commun Biol 2 (2019) 144.

[23] J. Teixeira, F. Basit, H.G. Swarts, et al., Extracellular acidification induces ROS- and mPTP-mediated death in HEK293 cells, Redox Biol 15 (2018) 394–404.

[24] A. Riemann, B. Schneider, A. Ihling, et al., Acidic environment leads to ROS-induced MAPK signaling in cancer cells, PLoS One 6 (2011), e22445.

[25] C. Zhu, W. Hu, H. Wu, X. Hu, No evident dose-response relationship between cellular ROS level and its cytotoxicity–a paradoxical issue in ROS-based cancer therapy, Sci. Rep. 4 (2014) 5029.

[26] J.A. Pan, Y. Sun, Y.P. Jiang, et al., TRIM21 ubiquitylates SQSTM1/p62 and suppresses protein sequestration to regulate redox homeostasis, Mol Cell 61 (2016) 720–733.

[27] Y.Y. Jin, H. Lin, L. Cao, et al., A convenient and biosafe replicon with accessory genes of SARS-CoV-2 and its potential application in antiviral drug discovery, Virol. Sin. 36 (2021) 913–923.

[28] D. Bartolini, A.M. Stabile, S. Bastianelli, et al., SARS-CoV2 infection impairs the metabolism and redox function of cellular glutathione, Redox Biol 45 (2021), 102041.

[29] H. Cha-Molstad, J.E. Yu, Z. Feng, et al., p62/SQSTM1/Sequestosome-1 is an N-recognin of the N-end rule pathway which modulates autophagosome biogenesis, Nat. Commun. 8 (2017) 102.

[30] M. Nag, K. Bera, S. Basak, Intermolecular disulfide bond formation promotes immunoglobulin aggregation: investigation by fluorescence correlation spectroscopy, Proteins 83 (2015) 169–177.

[31] D.E. Gordon, G.M. Jang, M. Bouhaddou, et al., A SARS-CoV-2 protein interaction map reveals targets for drug repurposing, Nature 583 (2020) 459–468.

[32] E. Lubos, J. Loscalzo, D.E. Handy, Glutathione peroxidase-1 in health and disease: from molecular mechanisms to therapeutic opportunities, Antioxidants Redox Signal. 15 (2011) 1957–1997.

[33] F. Hou, L. Sun, H. Zheng, B. Skaug, Q.X. Jiang, Z.J. Chen, MAVS forms functional prion-like aggregates to activate and propagate antiviral innate immune response, Cell 146 (2011) 448–461.

[34] Z. Wang, H. Jiang, S. Chen, F. Du, X. Wang, The mitochondrial phosphatase PGAM5 functions at the convergence point of multiple necrotic death pathways, Cell 148 (2012) 228–243.

[35] J.A. Pan, E. Ullman, Z. Dou, W.X. Zong, Inhibition of protein degradation induces apoptosis through a microtubule-associated protein 1 light chain 3-mediated activation of caspase-8 at intracellular membranes, Mol. Cell Biol. 31 (2011) 3158–3170.

[36] Y. Li, L. Cao, G. Li, et al., Remdesivir metabolite GS-441524 effectively inhibits SARS-CoV-2 infection in mouse models, J. Med. Chem. (2021).

[37] J.A. Pan, Y. Fan, R.K. Gandhirajan, M. Madesh, W.X. Zong, Hyperactivation of the mammalian degenerin MDEG promotes caspase-8 activation and apoptosis, J. Biol. Chem. 288 (2013) 2952–2963.

[38] S. Pankiv, T.H. Clausen, T. Lamark, et al., p62/SQSTM1 binds directly to Atg8/LC3 to facilitate degradation of ubiquitinated protein aggregates by autophagy, J. Biol. Chem. 282 (2007) 24131–24145.